# DEVELOPMENT OF AN ANALYTICAL FRAMEWORK FOR STRENGTH ASSESSMENT OF CORRODED STEEL BRIDGES

**Georgios Tzortzinis**

**Brendan T. Knickle**

**Simos Gerasimidis, PhD**

## BIOGRAPHIES

George Tzortzinis is a PhD candidate at the University of Massachusetts, Amherst. He received his Diploma in Civil Engineering from the University of Patras and his MSc degree in Computer Modelling and Finite Elements in Engineering Mechanics from Swansea University.

Brendan Knickle is a Structural Engineer at CME Associates, Inc serving as support to bridge design and consulting projects. Prior to joining the industry, he received an MSCE and BSCE from the University of Massachusetts Amherst.

Dr. Simos Gerasimidis is an Assistant Professor at the Department of Civil and Environmental Engineering at the University of Massachusetts, Amherst. He has worked as a Post-Doctoral Research Scientist at the Department of Civil Engineering and Engineering Mechanics of Columbia University. He received his Ph.D. from the Department of Civil Engineering of Aristotle University of Thessaloniki and his MEng from the Department of Civil and Environmental Engineering at MIT.

## SUMMARY

The national highway system consists of almost 55,000 structurally deficient bridges with corrosion as a common cause for steel viaduct deterioration. This condition can be primarily attributed to malfunctioning deck expansion joints, which fail to prevent water or deicing mixtures from penetrating into bearing area. The build-up of this runoff triggers a corrosive process which significantly varies in topology and intensity leading in many cases to severe section loss. This study aims to provide procedures for strength assessment of un-stiffened rolled I-beams with corroded ends.

The current deterioration condition of steel bridges in Massachusetts is first studied using MassDOT inspection reports of bridges that had experienced beam end corrosion. To better estimate strength of deteriorated components, full-scale laboratory testing of in-service corroded girders, obtained from bridge demolition projects in the state of Massachusetts, is performed. Making use of the test results, a calibrated numerical model capable of predicting the failure load during the tests is developed. Combining the corrosion patterns identified during the first part of the work with finite element modeling, an extensive numerical analysis is performed. Based on the numerical outcome, the current load rating procedures are evaluated and improvements are proposed.

**Alexander Bardow**

**Sergio F. Breña, PhD**

## BIOGRAPHY

Alexander Bardow, P.E., is the State Bridge Engineer for the Massachusetts Department of Transportation. He received both his BSCE and MSCE degrees in Civil Engineering from MIT. He is a voting member of the AASHTO Committee on Bridges and Structures and serves on various of its technical committees. He is also active in the National Cooperative Highway Research Program, serving on several of its project panels.

Sergio F. Brena, M. ASCE, FACI is a Professor of Civil and Environmental Engineering at the University of Massachusetts Amherst. His research interests include design and behavior of reinforced and prestressed concrete structures, use of fiber-reinforced materials in civil infrastructure applications, and field performance of bridges and buildings. He has over 20 years of experience in laboratory and field testing of structures and 6 years of structural design experience.

# INTRODUCTION

Approximately 40% of the roughly 600,000 bridges included in the National Bridge Inventory have been in service for more than 5 decades [1]. An unavoidable result of their aging is the deterioration of their assets. Deck expansion joints are high on the list with the most vulnerable components, as they are permanently exposed to natural and human originated deterioration factors. Malfunctioning joints fail to prevent water or deicing chemicals from penetrating into the superstructure and consequently at the load carrying components. For bridges made of steel girders, the build-up of this runoff triggers a corrosive process afflicting the as-designed dimensions of the elements at the support area. Topologically non-uniform and highly uncertain, the appearance of corrosion makes the residual bearing capacity quite challenging to be accurately assessed by inspectors and engineers.

The goal of this research work is to investigate and ultimately improve the efficiency and accuracy of the current procedures for strength assessment of corroded beam ends. In detail, real corrosion data are implemented in every aspect of the proposed methodology aimed at simple span and unstiffened above-bearing rolled girders, which are commonly found in the Commonwealth of Massachusetts.

The first part of this work focuses on the identification and quantification of the most common corrosion topologies. The second part experimentally assesses the residual loading capacity of naturally corroded beam ends obtained from bridge demolition projects in the state of Massachusetts. The third part implements the experimental data for the calibration and validation of a girder level finite element model able to capture the failure load and mode of the corroded beam ends. Next parametric analysis is initiated to study the factors that affect the load carrying reduction. Finally, at the fourth and last part of this study, empirical equations are provided based on the current MassDOT policies for capacity assessment of corroded beam ends.

# PART I: CORROSION PATTERNS

The current deterioration condition of 93 steel bridges throughout the state of Massachusetts is explicitly studied [2]. In order to manage the large amount of data included in these reports the first stage of processing involves the development of raw data-based patterns for web corrosion (Figure 1) as well as patterns of web holes (Figure 2) that describe the 95% of the reported cases. Each one of the 808 studied corroded beam ends is classified according to raw data based patterns and parameters such as thickness loss, corrosion area size, corrosion location, hole size, and hole location were clearly defined and recorded from the reports.

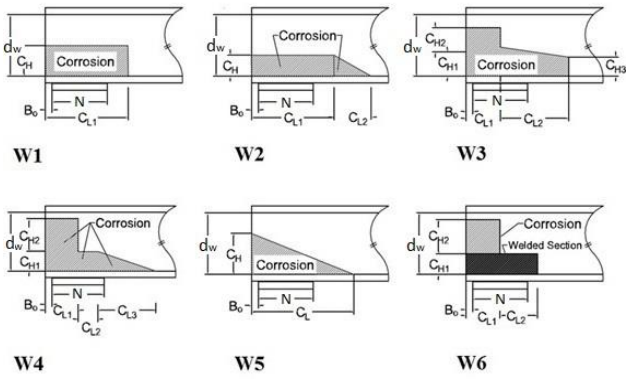


**Figure 1:** Raw data-based section loss patterns.

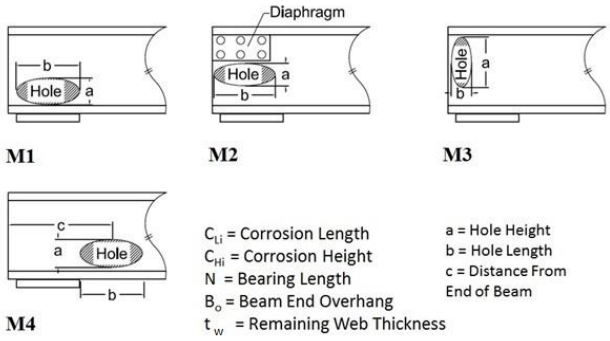


**Figure 2:** Raw data hole patterns.

The second stage of processing involves statistical analysis on the recorded data, the bounds of the most common corrosion topologies are quantified and reported for two broad categories: beams with and

without diaphragms above the bearing. Figure 3 shows the upper bounds of patterns for beams without diaphragms. The corrosion scenarios involve flange and web thickness reduction as well as web holes. For each one of the different topologies, the upper and lower bounds of every necessary geometric variable have been accurately defined.

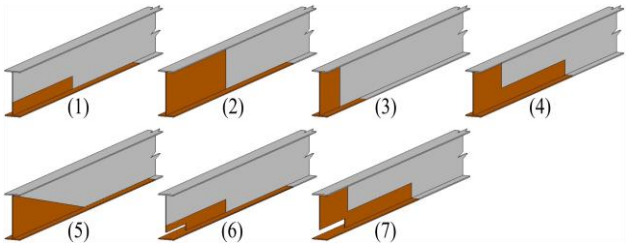


**Figure 3:** The most common corrosion patterns for beams without diaphragms above bearing.

For each one of the final corrosion pattens 1, 2 and 3 that will be implemented at later stages of this study, the associated parameters for web corrosion and their bounds are defined in Table 1.

**Table 1:** Analytical description of final corrosion patterns 1, 2 and 3 in Figure 3.

| Pattern | (1) | (2) | (3) |
|---|---|---|---|
| CH (dw) | (0, 0.3] | 1 | [0.15, 1] |
| CL (dw) | (0, 1.5] | [1, 1.5] | (0, 0.5] |
| $t_w$ ($_{tweb}$) | [0.2 0.8] | [0.8, 0.6] | [0.8, 0.6] |

# PART II: EXPERIMENTAL WORK

Other researchers have previously approached beam end corrosion from multiple perspectives, from evaluating the residual bearing capacity to developing innovative repair techniques. Except for the work of Sugimoto et al. [3] on railway bridges, all previous efforts have artificially introduced corrosion as a uniform thickness reduction on intact beams. It is considered quite challenging to gain access to naturally corroded beams for testing. In the real conditions of the field however, the deterioration phenomenon is rather non uniform, it varies significantly in topology and intensity and it is highly related to the configuration of the bearing area. Parameters like the type of bearing, the existence of a diaphragm as well as the position of the leaking deck joints directly affect the water flow resulting to a multi-variable parametric space. Thus, simulating corrosion as a uniform thickness reduction, potentially leads to results that are not realistic.

## Naturally Corroded Specimens

The research at UMass Amherst involves full-scale experimental testing on six naturally corroded girders [4] (numbered as specimens 1 to 6 from now on) obtained from two steel bridges built in 1939 in the state of Massachusetts that were undergoing replacement. Specimens 1 to 3 were obtained from the five span bridge from site A, which will be referred from now on as Bridge A; specimens 4 to 6 were obtained from the simple span bridge at site B, which from now on will be referred as Bridge B.

**Figure 4:** In-service configuration of Bridge A.

While Bridge A was in service, concrete diaphragms were located at the upper part of the web ends (Figure 4). Concrete removal revealed three artificial holes at each specimen as well as a skew cut of the upper web end and flange. Part of the steel angle sections utilized to support the diaphragms remained bolted at web mid-height.

Specimen 1 is a 332 in. long 33WF125 beam with extensive section loss along the corroded end (Figure 7). The defining characteristic of this specimen is the 6 in. long hole located above the bottom flange, extending along the 50% of the bearing length.

Specimen 2 is a 287 in. long 33WF132 beam with extensive section loss along the lower part of the

web end. It is worth noting that the maximum initial lateral web deviation (1.58 in.) from the vertical equals 2.7 times the intact web thickness ($t_{web}$).

Specimen 3 is a 335 in. long 33WF125 beam with two holes at the corroded end. The first one is 3 in. long located mid-height, and the second one is 18 in. long initiating from the outer edge of the web, extending 6 in. beyond the bearing length.

The design of Bridge B consisted of beams with their ends fully embedded in concrete along their depths (Figure 5). Concrete removal also revealed holes at the web end of specimens 4 to 6.

**Figure 5:** In-service condition of a girder in Bridge B.

Specimen 4 is a 272 in. long 21WF73 beam which has an area with extensive thickness loss at the bottom of the web extending in parallel with the flange. This specimen was delivered bent along the transverse axis of the web close to midspan.

Specimen 5 is a 241 in. long 21WF73, which has three corrosion generated web holes above the bearing. Holes have lengths from the bottom to the top of 8 in., 0.6 in. and 5 in.

Specimen 6 is 241 in. long 21WF59 beam with one hole extending vertically along the web depth, while it extends longitudinally close to both flanges.

## Experimental Test Setup

An experimental rig is designed to generate high shear and low moment. By observation of inspection reports provided by MassDOT, it is noticed that the majority of the Commonwealth's structurally deficient bridges were built between 1940 and 1980. According to the construction drawings of these bridges, the steel beams were typically not composite. Shear studs were not implemented to promote interaction between the steel beam and the concrete deck, although in some cases the top flanges of the beams were encased in the deck. This encasement covered just the thickness of the top flange, and it is therefore controversial how much composite action can be developed. Based on the non composite design assumption, a deck slab was not cast onto the girder prior to testing. However, the lateral support provided to girders is replaced by braces at a distance less than the buckling length. The cantilevered braces are placed every 5 ft (Figure 6) along the length of the specimen, with C channels bolted on the top in contact with specimen's top flange. This configuration prevents lateral torsional buckling while it ensured that web buckling occurred in the corroded region of interest. Specimens are simply supported by a pair of bearing plates.

The loading configuration is designed to stay within the force limitations of the laboratory's strong floor. It consists of two 60-ton through-hole jacks, placed in parallel, applying load to the specimen's top flange through a cross beam. The cross beam is designed to allow passage of a threaded rod that was anchored to the strong floor. In terms of this study, the beam end closer to the applied load is referred to as the corroded end, while the other end is the intact one. This configuration served two purposes: first, it ensured that the failure is shear dominated, and second, more than 75% of the load is distributed to the studied end.

## Instrumentation Configuration

The maximum beam deflection is measured using a linear variable displacement transducer (LVDT) installed on the outer face of the bottom flange beneath the point of load application. Eight potentiometers are used to measure the out of plane displacements at the corroded end. The potentiometers are installed on a frame, which allowed for placement of the instruments in an arrangement of two columns and four rows. This configuration is chosen in order to record two different sets of out of plane displacements taken over the height of the web. The first column of instruments is placed above the inner edge of the bearing, and the second one above the outer edge of

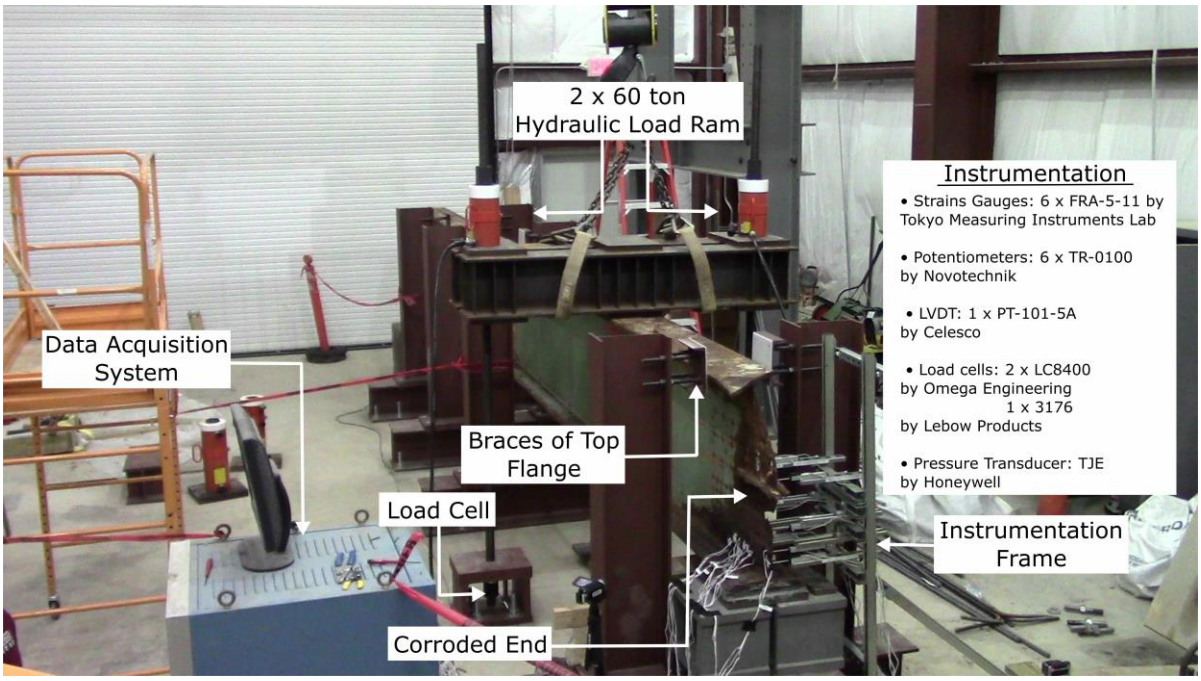


**Figure 6:** Experimental and instrumentation configuration.

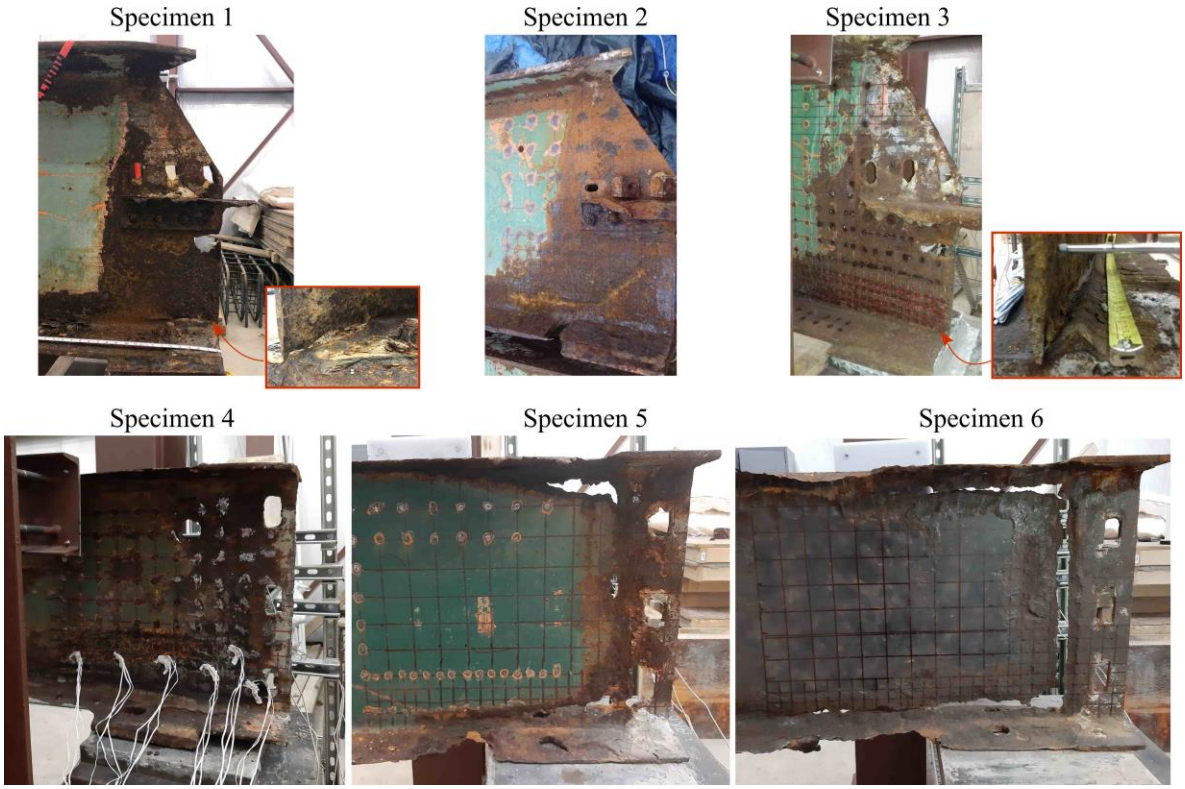


**Figure 7:** Tested specimens.

the bearing. At each specimen six strain rosettes are attached to the corroded web and flange to measure the strains. The rosettes are primarily installed at the area above the inner edge of the bearing. Finally, a pressure transducer is installed to monitor pressure in the hose downstream of the hydraulic pump.

## Section Loss Measurements

One of the main challenges is the accurate representation of the uneven section loss in the corroded end region. Detailed thickness measurements are performed along the corroded ends to accurately determine thickness loss throughout the corroded region. For ease of reference, a grid was drawn at each specimen. Moving from top to bottom, the grid increases in resolution (from 16 $in^2$ to 1 $in^2$), as visual inspection indicates the section loss to be most severe towards the bottom flange. Data are gathered using a Pocket Mike Compact Thickness manufactured by GE Inspection technologies [5].

## Experimental Results

Table 2 summarizes the experimentally obtained load capacities as well as a comparison with the predicted failure loads according to the current MassDOT provisions [6]. Figure 8 presents the initial condition and the residual deformation for each specimen.

Out of the six experiments, one is found 51% lower than the prediction, four are significantly underestimated by the current procedures, while for specimen 4, the failure of the corroded end is not reached due to a beam long-wave instability mode. From these results, a first conclusion is that the current manual procedures underestimate in some cases the actual capacity and overestimate it in others. It is impossible to overwhelmingly conclude between the two, as there is evidence for both conditions.

The failure mechanism of specimen 2 reveals one of the most important findings of the experimental program. The failure mode is strongly affected by the initial web's deviation from vertical. This type of imperfection is not currently considered in the MassDOT Manual procedures, and that is the reason that the procedures overestimated the capacity of this beam. This test was particularly important, since it showed that this initial lateral web imperfection severely affects the capacity of the beam end.

**Table 2:** Comparison between the experimental and the predicted bearing loads according to MassDOT procedures for 36 ksi steel.

| Specimen No | Experimental Capacity (kip) | MassDOT Prediction (kip) |
|---|---|---|
| 1 | 99.1 | 38.3 |
| 2 | 67.6 | 102.2 |
| 3 | 84.3 | 0 |
| 4 | 42.8 | 91.5 |
| 5 | 30.9 | 17.6 |
| 6 | 40.9 | 6.1 |

# PART III: COMPUTATIONAL WORK

Initially, a high fidelity numerical model capable of predicting the capacity of beam ends is developed. Then the developed model is implemented to study parameters that affect the residual bearing capacity.

## Finite Element Model

The experimentally obtained data are implemented to provide a girder level finite element model. The model is calibrated based on the experimentally obtained data of specimen 1 and subsequently it is implemented to simulate specimen 2 and to validate the experimentally obtained results.

Regarding the mechanical model formulation the exact dimensions of both specimens are simulated. The primary challenge for a realistic geometric representation is the simulation of the irregular corrosion damage. Based on the thickness measurements, points with similar section loss are grouped together forming areas with common thickness reduction. Holes are also surveyed and included in the models. Steel material properties are defined by performing tensile tests on coupons extracted by specimen 1. Both specimens were manufactured in the same period and they were part of the same span. Thus, material properties from specimen 1 are considered representative for both specimens.

Finally, the boundary and loading conditions replicate the experimental configuration. The load is applied downwards as uniform pressure on a 18 in. long domain covering the full width of the top flange, similar to the actual contact area with the cross beam in Figure 6. The out of plane

displacement of the top flange is not allowed at the locations of the LTB restrictions. The beam is resting on a bearing plate at each end.

The commercial finite element software ABAQUS [7] is utilized for simulation and analysis of the conducted experiments. Shell elements are employed to approximate the three-dimensional continuous body with a surface at the middle of the section. The initial web lateral deviation from straightness is introduced in the models based on the eigenmode shapes. Each model is initially solved using an eigenvalue buckling analysis algorithm and the eigenmodes that better match the shape of the actual specimens are introduced as an initial geometric imperfection for the quasi-static analysis, scaled to the measured maximum lateral deviation of the web (1 $t_{web}$ and 2.7 $t_{web}$ for specimens 1 and 2 respectively, where $t_{web}$ is the intact web thickness of each specimen).

The most challenging part of the model is the simulation of the interaction between the bottom flange and the bearing plate. An infinitesimally stiff interaction ("hard contact") along the normal direction, instantly results to a hinge formulation (Figure 9) along the inner bearing edge deviating from the actual behavior. Thus, a stiff but "softened contact" is preferred. The interaction is defined using a linear contact pressure - overclosure relationship "k".

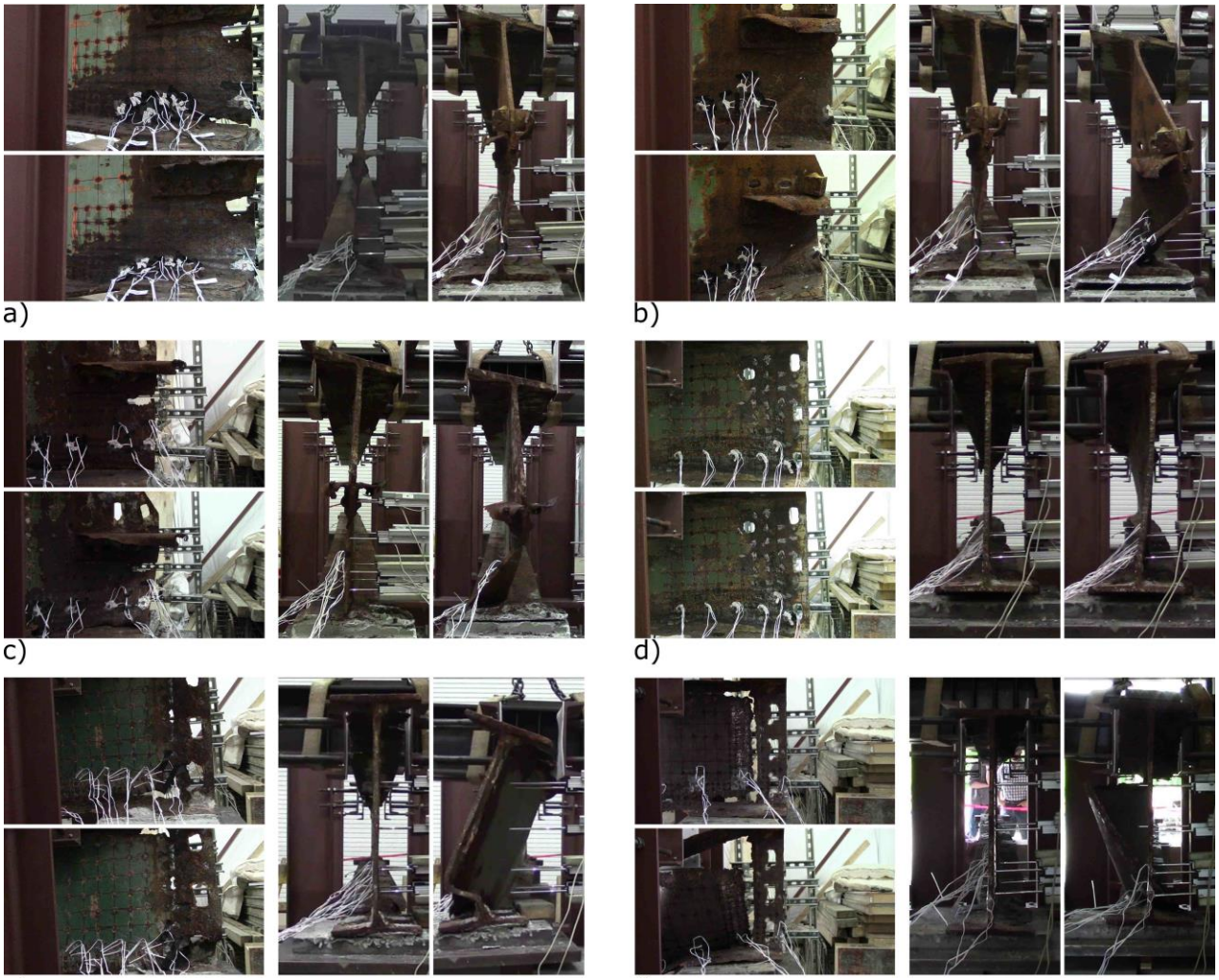


**Figure 8:** Side and front view of the initial and residual deformation for specimens a) 1 to f) 6.

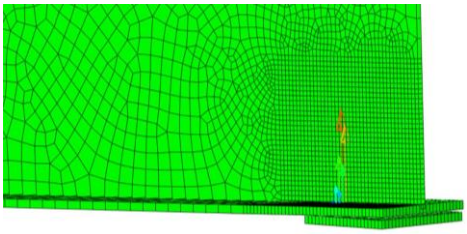

**Figure 9:** Hinge formulation for hard contact.

The only parameter which requires calibration is the "k" value, that has been set equal to 12 using the experimental data from specimen 1. The developed model is able to capture the failure mode of specimen 1 with accuracy of 3.5% (Figure 10a).

Following the procedure previously described specimen 2 was also simulated and analyzed using "k" equals 12. Both the stiffness and the peak load depict an excellent agreement between the experimental and numerical results. The numerically captured applied failure load overestimates the actual one by only 1.1% (Figure 10b).

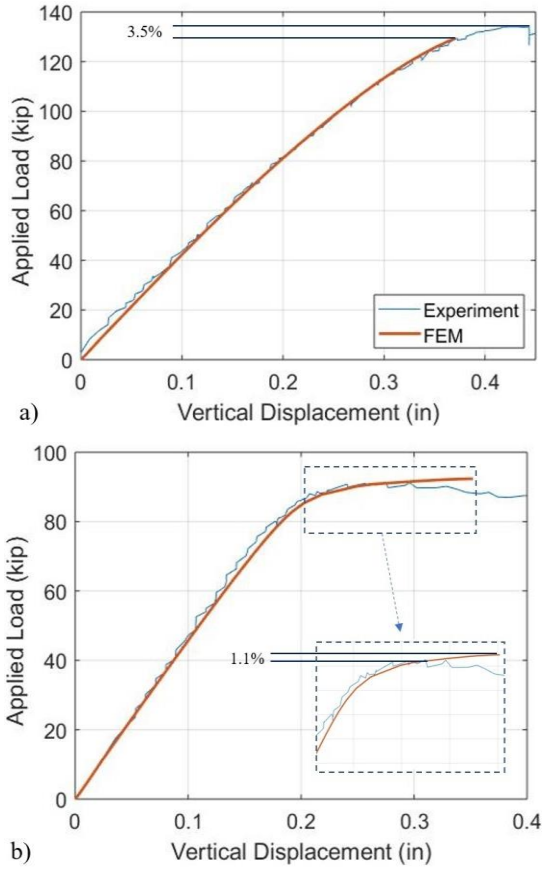


**Figure 10:** Comparison between experimental and numerical results for a) specimen 1 and b) specimen 2.

# Parametric Analysis

The developed model is employed to a series of analysis to gain fundamental understanding of the deterioration impact on the I-beam capacity under the assumption of uniform section loss.

The experimental part of this work highlighted that in-service beams are not perfectly straight. The cross section may deviate from the ideal shape as well the member's center line for its straightness. This observation triggered the numerical investigation to explore the effect of deviation magnitude on the bearing capacity.

Figure 11 shows the relationship of the initial imperfection amplitude (or maximum web deviation from straightness) and the bearing capacity for a 36WF150 beam with a corroded end. The nominal capacity based on [6] is also included for a comparison between the numerical results and the current Bridge Manual procedures. For the presented scenarios the bearing failure load is reduced up to 43% for imperfection amplitude equal to two times the intact web thickness.

Additional analyses are run to examine the effect of corrosion characteristics to the residual strength of deteriorated beam ends. Based on the previous findings, results are presented for imperfection amplitudes in the range of 0.1 $t_{web}$ to 1 $t_{web}$. Figure 12 reveals that for an orthogonal shaped damage area and imperfection amplitude 1 $t_{web}$, a corrosion domain extending beyond the 30% of web depth ($d_w$) has no significant impact on the bearing capacity (Figure 12a), as the extensive web lateral dislocation dominates the failure. On the other hand for reduced initial imperfection amplitudes, increasing corrosion height (CH) results in reduced bearing capacity (Figure 12b).

A similar procedure is followed to examine the effect of corrosion length (CL). According to Figure 13 there is a strong association between the initial web imperfection and the length of the damage area that significantly affects the bearing capacity.

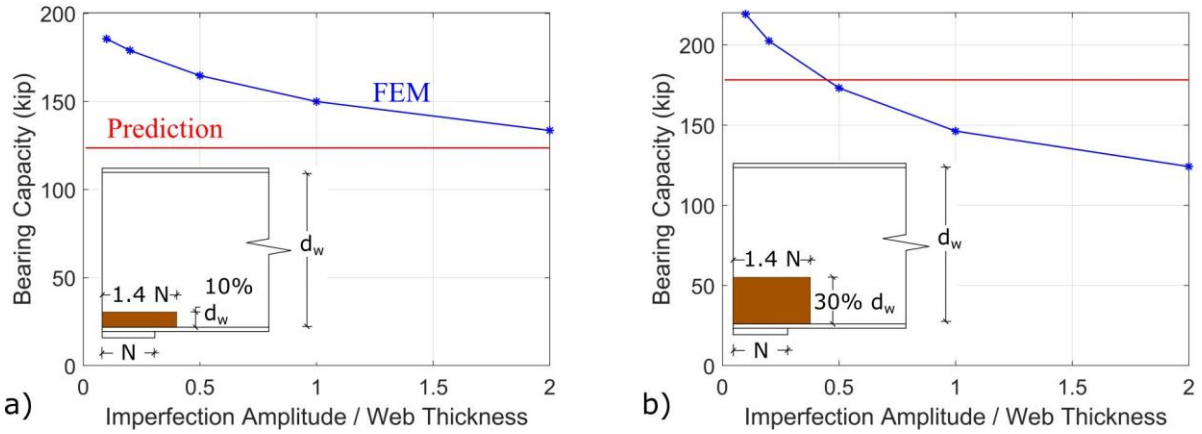


**Figure 11:** Effect of initial imperfection amplitude on the residual bearing capacity for section loss a) 45% and b) 25% of intact web thickness. Corrosion domain is illustrated with brown color.

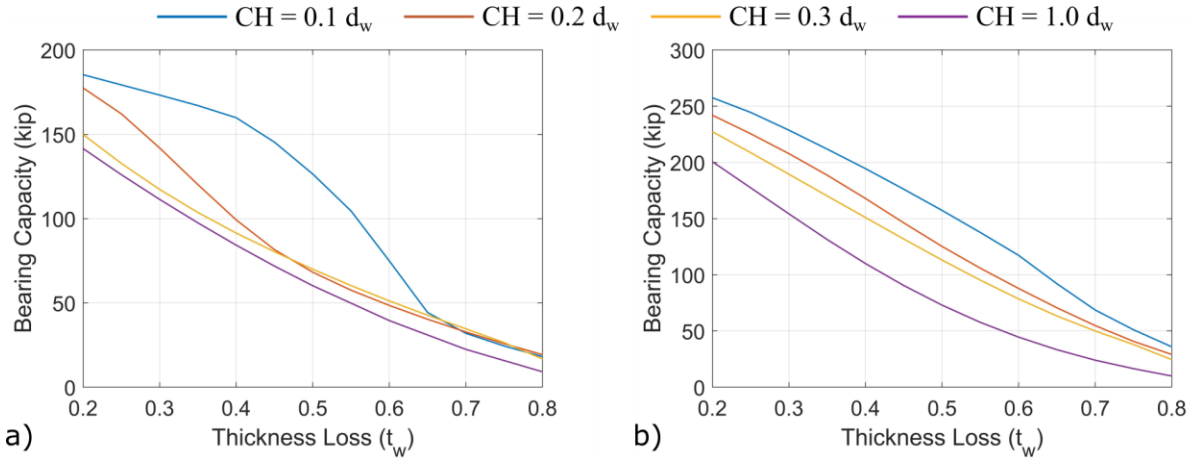


**Figure 12:** Effect of corrosion height (CH) for imperfection amplitude a) 1 $t_{web}$ and b) 0.1 $t_{web}$.

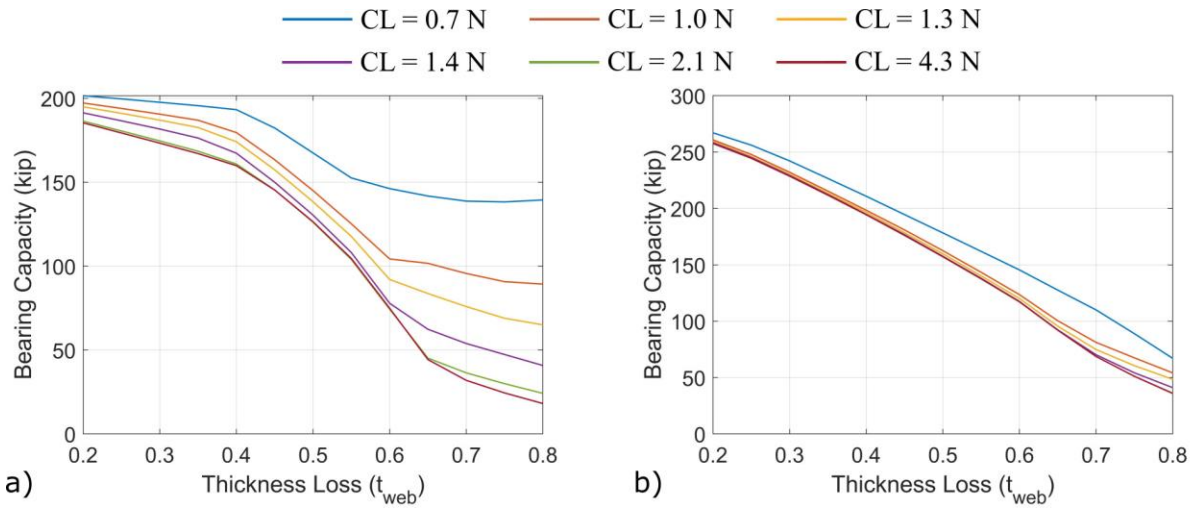


**Figure 13:** Effect of corrosion length (CL) for imperfection amplitude a) 1 $t_{web}$ and b) 0.1 $t_{web}$.

# PART IV: PROPOSED PROVISIONS

The proposed provisions emerge from the relationship between corrosion characteristics and bearing failure load of a sample consisting of more than 1300 simulated scenarios. These scenarios describe corrosion topologies within the range of variability of patterns 1, 2 and 3 in Table 1, for two imperfection amplitudes 0.1 $t_{web}$ and 1 $t_{web}$. The finite element models are created by implementing an in house developed Python script, which operates through ABAQUS software, assembling suitable meshes.

Modified empirical equations are developed from the current crippling equations presented in [6] for beams with overhang length less than 5k. k is the distance from the outer face of the flange to web toe fillet, as defined in [8]. The proposed equations aim to create envelopes for both captured failure modes, crippling and buckling. However the nominal ultimate bearing load should be estimated as the minimum between the proposed crippling and yielding equation as it currently exists in [6].

The proposed modifications are focusing on 4 main aspects: the initial imperfection amplitude, the area over which the average web thickness is determined, and finally the crippling capacity equations for varying N/d ratios (N denotes the bearing length and d the beam depth).

## Initial Imperfection Amplitude

The proposed procedures are developed for two different imperfection amplitudes, denoted as $\alpha$, which equal to 0.1 $t_{web}$ and 1 $t_{web}$.

## Average Web Thickness

The corrosion contribution to capacity reduction is considered by defining the average web thickness $t_{ave}$, which is calculated within a domain at the bottom 4 in. of the web, with length $N + md$ (the $m$ factor is given in Table 3) from the web edge, according to Equation 1.

$$t_{ave} = \frac{(N+md-H)t_w}{N+md} \quad (1)$$

Where:

$t_w$: remaining web thickness (in.)

$H$: length of hole along length used for capacity (here: $N+md$ ) (in.)

$N$: bearing length (in.)

$d$: beam depth (in.)

$m$: factor specified in Table 3.

**Table 3:** Proposed values of factor m.

| Imperfection Amplitude (a) | 1 $t_{web}$ | 0.1 $t_{web}$ |
|---|---|---|
| N/d > 0.2 | 0.2 | 0.1 |
| N/d ≤ 0.2 | 0.1 | 0 |

## Capacity equation for N/d > 0.2

The current crippling equations are modified to the following form:

$$R_n = [\, A\sqrt{E\,F_y\,t_f}\,t_{ave}^{1.5} + B^{\left(\frac{0.33d}{N}\right)}\left(\frac{4\,(N-H)}{d} - 0.2\right)\frac{\sqrt{E\,F_y t_f}}{t_f^{1.5}}\,t_{ave}^3\left(\frac{CL}{N+md}\right)^h \quad (2)$$

Where:

$E$: Young's Modulus

$F_y$: yield stress

$t_f$: flange thickness

$CL$: Corrosion length within $N+md$

$A$, $B$, $h$: Coefficients specified in Table 4.

**Table 4:** Proposed coefficients for Equation (2).

| Imperfection Amplitude (a) | 1 $t_{web}$ | 0.1 $t_{web}$ |
|---|---|---|
| A | 0.37 | 0.57 |
| B | 0.17 | 0.23 |
| h | 0.1 | 0.4 |

## Capacity equation for N/d ≤ 0.2

The current crippling equations are modified to the following form:

$$R_n = [\, C\sqrt{E\,F_y\,t_f}\,t_{ave}^{1.2} + D\left(\frac{(N-H)}{d}\right)\frac{\sqrt{E\,F_y\,t_f}}{t_f^{1.5}}\,t_{ave}^3]\left(\frac{t_{ave}}{t_{web}}\right)^h \quad (3)$$

Where:

$t_{web}$: Intact web thickness

C, D: Coefficients specified in Table 5.

**Table 5:** Proposed coefficients for Equation (3).

| Imperfection Amplitude (a) | 1 $t_{web}$ | 0.1 $t_{web}$ |
|---|---|---|
| C | 0.33 | 0.38 |
| D | 0 | 0 |
| h | 0.4 | 0.15 |

# Validation of proposed provisions

The beams tested in this research study had a variety of deterioration at their ends. Out of the six specimens tested in this project, five of them had holes in their deteriorated end. The new procedures proposed as a result of this research project have not focused on alternating the approach to hole inclusion in the methodology for the prediction of the capacity of deteriorated ends, and therefore, the impact of the new procedures for these specific cases is estimated to be minimal. The only specimen that did not have a hole was specimen 2, and for that reason only, this specimen is presented in this section.

**Table 6:** Comparison between experimental and predicted capacities for specimen 2.

| | Experimental | Current Procedures | Proposed Procedures | Difference |
|---|---|---|---|---|
| Capacity (kip) | 67.6 | 102.2 | 81.2 | -21% |

The proposed methodology reduces the discrepancy between the experimental and the estimated capacity that emerges from the flange hole as well as the extensive initial web displacement. The efficiency of the new prediction is demonstrated in this example, due to the fact that there is no hole in this specimen. However, the new procedures still overestimate the capacity. This is attributed to the extensive imperfection that cannot be accounted for, even with the new procedures (2.7 $t_{web}$)

In order to evaluate the efficiency of the proposed equations, the failure loads of a large number of scenarios coming from the numerical models were compared to the new procedures. Due to the size of the data (more than 1.300 models were used), indicative examples of these comparisons will be presented here. In addition to that comparison, the predictions of the current procedures are also included in the Figures 14 and 15.

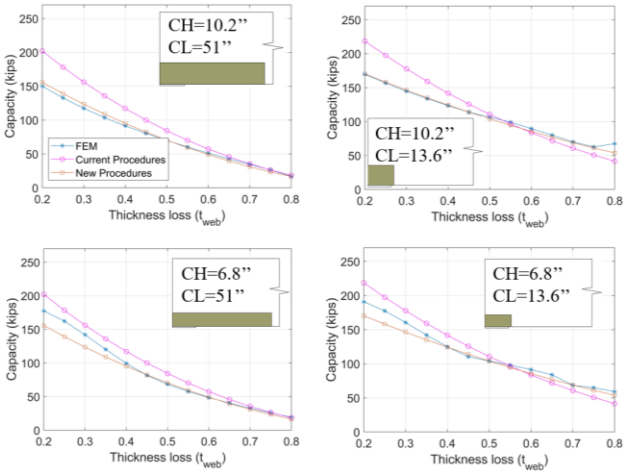


**Figure 14:** Comparison between numerically obtained capacities and failure load predictions based on current and proposed procedures, for $N/d$=0.33 and imperfection amplitude $t_{web}$.

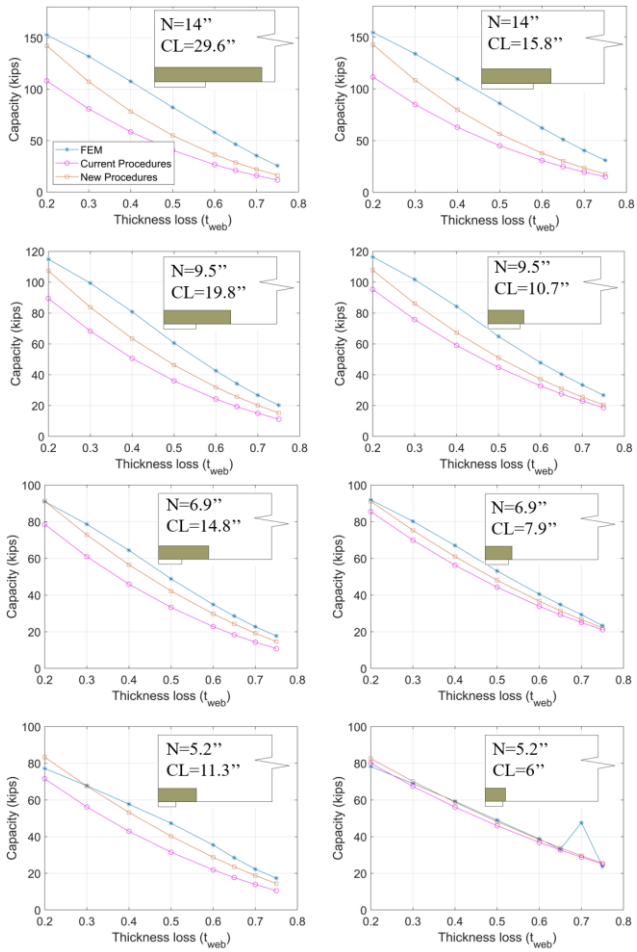


**Figure 15:** Comparison between numerically obtained capacities and failure load predictions based on current and proposed procedures, for a

variety of *N/d* ratios, *CH* = 20% *dw* and imperfection amplitude 0.1 $t_{web}$.

The presented results offer strong evidence that the proposed procedures provide a more accurate estimation of the actual capacity of corroded beam ends.

# CONCLUSIONS

This study aimed to address the residual capacity of unstiffened steel beams with corroded ends. Initially the current deterioration condition of 93 steel bridges in the state of Massachusetts was studied in detail. Corrosion patterns which summarize the most common deterioration topologies were defined and quantified.

This study was the first that tested naturally corroded specimens obtained from two different highway bridge demolition projects in the Commonwealth of Massachusetts. The research team tested six beams that spanned at least 20 ft., with 33 in. and 22 in. depths and reported the peak failure loads.

The failure mechanism of specimen 2 revealed one of the most important findings of the experimental program. The failure mode was strongly affected by the initial lateral web imperfection. This type of imperfection is not currently considered in the Manual procedures, and that is the reason that the current MassDOT procedures overestimated the capacity of this beam.

The experimental data were used to calibrate and validate a finite element model which captured the failure load of specimens 1 and 2 with accuracy 3.5% and 1.1% respectively. Consequently, it was implemented in a series of analysis to study the effect of different corrosion parameters on the residual bearing capacity, under the assumption of uniform section loss. The numerical results also confirmed the deleterious effect of the initial web deviation from plumbness, without to conclude which corrosion scenarios are underestimated by the current procedures and which not. The effect of corroded area dimensions (height and length) on the capacity reduction were found to be strongly related to the initial web imperfection.

Finally, new procedures were proposed for strength evaluation of unstiffened rolled I-beams with corroded ends. The current procedures were modified to better reflect the outcome of more than 1,300 simulated and analyzed corrosion scenarios for two different imperfection amplitudes (0.1 *tweb* and 1 *tweb*). This approach highlights the need for inspectors to document the amount of web deviation from straightness.

# ACKNOWLEDGEMEMENTS

This study was undertaken as part of the Massachusetts Department of Transportation Research Program with funding from the Federal Highway Administration State Planning and Research funds, under the Project (ISA: INTF0OXO2O18H0100519). The authors are solely responsible for the accuracy of the data, the validity of the analysis, and the views presented herein.

# REFERENCES

1. American Society of Civil Engineers. 2017. “2017 Infrastructure report card.” Accessed December 15, 2019. https://www.infrastructurereportcard.org/.
2. Tzortzinis, G., Knickle, B., Gerasimidis, S., Bardow, A., S. Breña. 2019. “Identification of most common shapes and locations for beam end corrosion of steel girder bridges.” In *Proc., 98th Annual Meeting of Transportation Research Board. Washington, DC: TRB.*
3. Sugimoto, I., Kobayashi, Y., and A. Ichikawa. 2006. “Durability evaluation based on buckling characteristics of corroded steel deck girders.” Quarterly Report of RTRI, 47(3): 150–155.
4. Tzortzinis, G., Knickle, B., Gerasimidis, S., Bardow, A., S. Breña. 2019. “Experiments and computations on steel bridge corroded beam ends.” In *Structural Stability Research Council. Chicago, IL: AISC.*
5. PocketMIKE. 2004. Operating manual. Lewistown, PA: GE Inspection Technologies.
6. Massachusetts Department of Transportation. 2019. Draft Bridge Manual Part I. Boston, MA: MassDOT.

7. Simulia. 2014. Abaqus user's manual.

   Providence, RI: SIMULIA

8. American Institute of Steel Construction. 2017 . Steel Construction Manual, 15th ed. Chicago, IL:AISC.